A balance between elastic and rigidified chromatin states regulates transcriptional plasticity at human centromeres

Daniël P. Melters[1,*], Tatini Rakshit[1,*], Mary Pitman[1,2], Minh Bui[1], Garegin A. Papoian[2], and Yamini Dalal[1,#]

1 National Cancer Institute, Center for Cancer Research,

Laboratory of Receptor Biology and Gene Expression, Bethesda, MD

2 University of Maryland, Department of Chemistry and Biochemistry, College Park, MD

* Contributed equally

Corresponding author: dalaly@mail.nih.gov

Summary

Histone variants fine-tune the regulation of transcription, replication, DNA damage repair, and cell division relies on distinct chromatin states. The histone H3 variant CENP-A/CENH3 seeds the kinetochore, creating the physical interface between centromeric chromatin and mitotic spindles. How kinetochore proteins modify CENP-A nucleosome dynamics and how these dynamics affect centromere chromatin states is poorly understood. Using interdisciplinary analyses, we report that CENP-A nucleosomes are intrinsically elastic, but CENP-C binding suppresses this innate elasticity. Shifting the balance between elastic and rigid CENP-A states *in vivo* results in the suppression of centromeric chromatin plasticity, so that centromeric chromatin becomes less permissive to RNA polymerase 2, thereby diminishing new CENP-A loading. These data suggest a link between innate structural properties possessed by histone variant

nucleosomes, and adaptability of chromatin states *in vivo*, which in turn dictate the transcriptional plasticity of the underlying locus.

Introduction

The adaptive nature of chromatin states allows a cell to replicate, divide, differentiate, transcriptionally respond to various stimuli, and repair damaged DNA[1,2]. In part, this dynamic chromatin landscape is shaped by removing old and incorporating new nucleosomes[3,4], by incorporating specific histone variants[5], and by incorporating covalent modifications[6-8]. How different histone variants convey unique biophysical properties of their nucleosomes to the chromatin fiber, and whether such non-canonical nucleosomes modulate chromatin dynamics remains a subject of intense studies.

One of the most striking cellular events is mitosis, when chromosomes condense into rod-shaped structures, temporarily yet dramatically changing the transcriptional landscape[9,10]. Chromosome segregation is a mechanical process, where chromosomes are actively pulled from the metaphase plate towards the poles[11]. This process relies, in part, on the presence of specialized centromeric nucleosomes. Epigenetically the centromere is marked by the enrichment of the histone H3 variant CENP-A/CENH3[12-16]. Despite lack of sequence conservation at the level of CENP-A or its associated DNA[12,17], in most species, CENP-A chromatin provides the foundation by recruiting a triad of inner kinetochore proteins: CENP-B, CENP-C, and CENP-N[18-21]. Deleting either CENP-A or CENP-C results in cell death or induces senescence[22,23]. This happens only after a few cell cycles, suggesting that both CENP-A and CENP-C are likely present in excess over that required to form a functional kinetochore for one cell cycle. While CENP-A and

CENP-C are long-lived proteins, guaranteeing faithful chromosome segregation even after their genes have been deleted[24-28], incorporation of new CENP-A in human cells depends strongly on the transcription of centromeres at the end of mitosis/early G1[27,29,30]. A major paradox is how active transcription, which normally requires accessible chromatin, is accomplished at a time when kinetochore-bound centromeric chromatin is engaged in completion of mitosis. Consequently, elucidating biophysical features of the inner kinetochore-associated chromatin, composed of CENP-A nucleosomes and its closest bound partners such as CENP-C, remains a fundamental biological question.

To investigate these questions, in this report, we used *in silico*, *in vitro*, and *in vivo* tools to dissect the dynamic nature of CENP-A nucleosomes compared to H3 nucleosomes, either with, or without CENP-C. Using all-atom molecular dynamic simulations, we report that when a CENP-A nucleosome is bound to CENP-C, its local and global flexibilities are severely limited, so that CENP-C fixes specific conformational states of a CENP-A nucleosome. To experimentally test the global changes of nucleosome dynamics, we directly measured the elasticity of CENP-A nucleosomes, finding to our surprise, that they are twice as elastic as H3 nucleosomes. Remarkably, upon CENP-C binding, CENP-A nucleosomes markedly rigidify by three-fold and cause three-dimensional compaction of centromeric chromatin fibers. *In vivo*, we demonstrate that CENP-A chromatin plasticity is required for recruitment of the transcriptional machinery. Indeed, overexpression of CENP-C led to overcompaction of centromeric CENP-A chromatin, reduced the levels of RNA polymerase 2 (RNAP2) occupancy at centromeres, which we show is concomitant with a reduction of *de novo* CENP-A loading in early G1. These data

support a model in which a balance between elastic and rigidified centromeric nucleosomes regulates the plasticity and fidelity of the centromeric chromatin fiber *in vivo*.

Results

CENP-A nucleosomes are highly elastic compared to H3 nucleosomes

Previous computational results found that CENP-A nucleosomes are conformationally distortable compared to canonical H3 nucleosomes[31]. One prediction from these experiments was that nucleosome distortability would correlate with nucleosome elasticity; in other words, the more deformable a nucleosome, the more likely it is to be elastic. Elasticity of materials is measured by the ratio of stress (N/m^2 or Pascal) to strain (indentation), known as the Young's modulus. In physics and biology, nano-indentation experiments are a well-accepted means of measuring the elastic properties of biological materials[32-34].

Despite the longstanding use of nanomechanical force spectroscopy, we were surprised to discover that the elasticity of nucleosomes of any kind, has never been reported. Therefore, we performed in-fluid, single-molecule, nano-indentation force spectroscopy[35,36] of canonical H3 and variant CENP-A nucleosomes within *in vitro* reconstituted arrays under physiological conditions (Figure 1A). As reported earlier[37,38], we found that *in vitro* reconstituted CENP-A nucleosomes possess dimensions similar to H3 nucleosomes (3.7±0.3 and 3.8±0.3 nm, resp.) (Table S1). Next, we performed in-fluid nano-indentation on these reconstituted nucleosomes (Figure 1A,B). H3 nucleosomes had a Young's modulus of 11.1±4.5 MPa. Strikingly, CENP-A nucleosomes were nearly twice as elastic (6.2±3.9 MPa, Figure 1B-D, Table S2) as H3 nucleosomes.

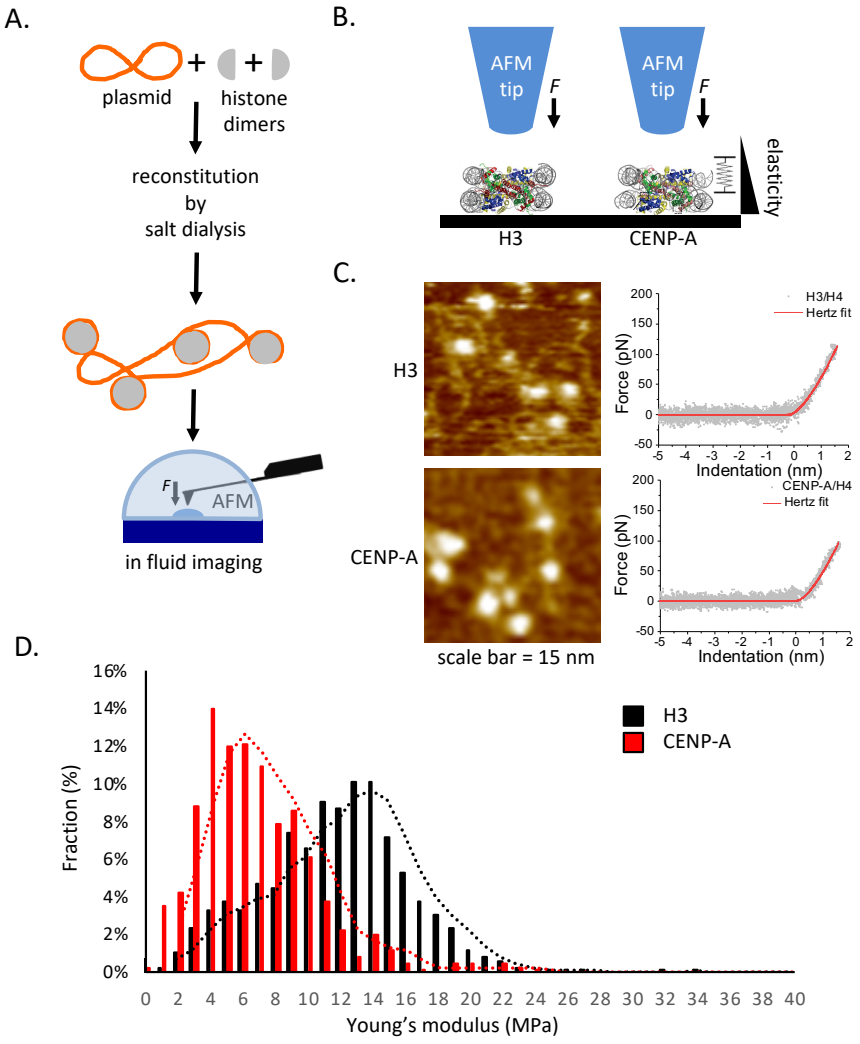

Figure 1. CENP-A nucleosomes are elastic

(A) To be able to determine the Young's modulus of CENP-A and H3 nucleosome arrays, we *in vitro* reconstituted these arrays by salt dialysis. (B) Graphical representation of nano-indentation force spectroscopy experiment for H3 and CENP-A nucleosomes. (C) Representative AFM images and force curves with Hertz model (spherical indenter) of reconstituted H3 and CENP-A nucleosomes. (D) Histogram and summary table of Young's modulus values showing that CENP-A nucleosomes are more elastic than H3 nucleosomes (ANOVA test $P<0.0001$).

Modeling CENP-A:CENP-C^{CD} nucleosomes predicts a change in conformational flexibility

These elasticity measurements are compatible with previous computational modeling results, which demonstrated that CENP-A nucleosomes have an intrinsically more distortable

nucleosome core, compared to H3 nucleosomes[31]. The corresponding free energy landscape predicts the existence of multiple conformational states of CENP-A. Next, we performed all-atom explicit-solvent molecular dynamics simulations with, or without the central domain fragment of CENP-C (CENP-C^{CD})[39-41], from which we obtained the free energy landscapes of CENP-A nucleosomes. Strikingly, in the presence of CENP-C^{CD}, the otherwise rugged free energy landscape of CENP-A nucleosomes collapses into just two broad basins (Figure 2A), with a distribution similar to that of H3[31]. This change in the free energy landscape manifested itself in the loss of the bimodal distribution of the movements of the center of mass (Figure S1A). Furthermore, local structural flexibility was also suppressed upon CENP-C^{CD} binding (Figure S1B). Overall, these findings indicate that CENP-C^{CD} limits the conformational distortability and motions of CENP-A nucleosomes.

Next, we computationally examined the effect of doubling the amount of CENP-C per CENP-A nucleosome. Compared to a single CENP-C^{CD} fragment, binding two CENP-C^{CD} fragments globally reduced whole histone motions and local residue fluctuations of CENP-A nucleosomes (Figure S2A, B). We also assessed DNA gyre sliding and gaping motions within the CENP-A nucleosome. We modeled these motions using the same residues as in previous smFRET experiments[33]. In support of these published experimental data, our high-resolution analysis showed that a single CENP-C^{CD} fragment dampened the CENP-A nucleosome gyre gaping; where DNA slides asymmetrically away from the CENP-C bound-face of CENP-A nucleosomes. In contrast, two CENP-C^{CD} fragments froze both, gaping and sliding motions (Figure 2B, S2C). One prediction from these modeling data is that increasing CENP-C concentration should dampen CENP-A nucleosomal plasticity in a dose-dependent manner.

CENP-C^{CD} rigidifies CENP-A nucleosomes

We were curious whether CENP-C^{CD} would suppress CENP-A nucleosomal elasticity. First, we measured the dimensions of CENP-C^{CD} bound to CENP-A nucleosomes, finding that they are slightly taller than CENP-A nucleosomes alone (3.7±0.3 nm vs. 4.1±0.4 nm) (Table S1). Next, we measured the Young's modulus. About half the CENP-A nucleosomes remained highly elastic (5 MPa), whereas the other half lost elasticity by a factor of three (14.5 MPa) (1-way ANOVA P<0.0001; Figure 2C-E, Table S2). This bimodal distribution of the CENP-A+CENP-C^{CD} population most likely represents two distinct CENP-A sub-species: one free (5 MPa), and the other bound to CENP-C^{CD} (14.5 MPa). When we doubled the amount of CENP-C^{CD}, virtually all CENP-A nucleosomes lose elasticity, and become rigidified (17.1±10.6 MPa, Figure 1D,E, Table S2) in a dose-dependent manner.

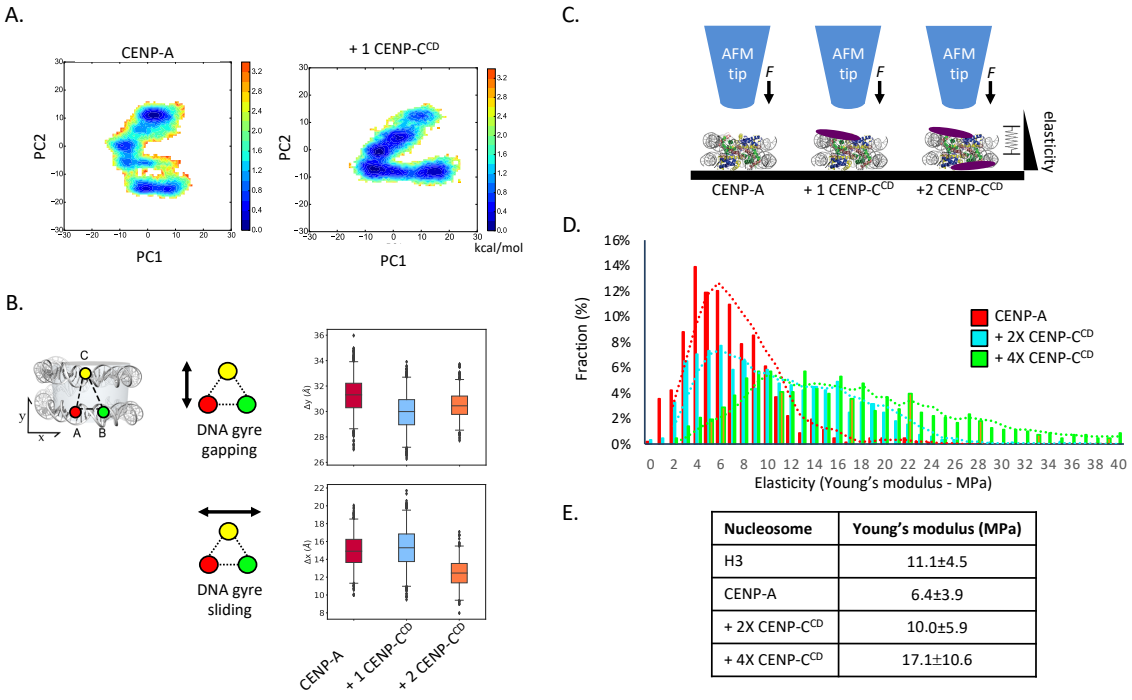

Nucleosome	Young's modulus (MPa)
H3	11.1±4.5
CENP-A	6.4±3.9
+ 2X CENP-C^{CD}	10.0±5.9
+ 4X CENP-C^{CD}	17.1±10.6

Figure 2. CENP-C^{CD} binding rigidifies CENP-A nucleosomes

(A) The free energy landscape of CENP-A nucleosomes alone or CENP-A nucleosome with CENP-C^{CD} fragment was determined by principle component analysis. CENP-A nucleosomes display a rugged free energy landscape, which is locked down when CENP-C^{CD} is bound, increasing the connectivity of the energetic minima. (B) All-atom computational modeling of DNA gyre gapping or DNA gyre sliding of CENP-A nucleosome alone or bound to either 1 or 2 CENP-C^{CD} fragments. (C) Graphical representation of nano-indentation force spectroscopy experiment for CENP-A nucleosomes alone and incubated in the presence of 2.2-fold or 4-fold excess CENP-C^{CD} fragment. (D) Histogram of Young's modulus values showing that CENP-A nucleosomes become rigidified upon addition of CENP-C^{CD} in a dose-dependent manner (ANOVA test $P<0.0001$). (E) Tabular representation of the Young's modulus for H3, CENP-A, CENP-A nucleosomes with 2.2-fold, or 4-fold excess CENP-C^{CD}.

Altering the balance between flexible and rigid CENP-A domains changes chromatin plasticity

These modeling and nano-indentation data support a model in which CENP-C fixes the elastic CENP-A nucleosome in a conformational state more similar to H3 nucleosome, and compact CENP-A chromatin. We were very curious to elucidate potential functions for elastic CENP-A nucleosomes and open vs. closed chromatin states *in vivo.*

We first hypothesized that during mitosis smaller CENP-A particles might provide a mechanical "bungee"-like state, which allows the dissipation of mitotic forces. In this scenario, we postulated, excess CENP-C would dampen the motions of CENP-A (Figure 2), thereby reducing the overall springiness of centromeric chromatin; and loss of the flexible CENP-A domain might result in an accumulation of DNA breaks during mitosis. To test this hypothesis, we transiently overexpressed C-terminally tagged GFP CENP-C (OE) for three days, in cells synchronized to late mitosis and early G1 (Figure 3A) and scored for the DNA break marker γH2A.X. Although

we do observe an increase in mitotic defects (Figure S3, no appreciable increase in γH2A.X was observed at centromeric foci (Figure S4). These data, *a priori*, do not provide evidence that flexibility of CENP-A plays a direct role in dissipation of mitotic tension.

A second hypothesis we considered was whether the flexible CENP-A domain provides an open chromatin state, permissive to transcription. This hypothesis is supported by the observation CENP-A chromatin cannot compact through H1 due to CENP-A's shorter αN helix which prevents DNA entry/exit cross-overs[42]. In this scenario, we postulated, excess CENP-C should compact the open chromatin state, thereby inhibiting the transcriptional machinery, namely, RNA polymerase 2 (RNAP2). In turn, because centromeric transcription has been shown to be critical for *de novo* CENP-A loading[43], compaction driven by loss of elasticity could result in loss of transcriptional potential, and thereby impact new CENP-A loading.

Indeed, *in vitro,* we noticed a qualitative increase in clustering of reconstituted CENP-A nucleosome when exposed to CENP-C. This phenomenon occurred in a dose-dependent manner (Figure S5A). We were curious to know whether we could induce CENP-A chromatin compaction simply by adding recombinant CENP-C^{CD} fragment to kinetochore-depleted CENP-A chromatin fraction. We purified bulk CENP-A chromatin from human cells and incubated these samples with our CENP-C for 30 minutes, followed by analysis of clustering. We observed a ~30% increase in chromatin compaction upon the addition of CENP-C^{CD} (Figure 3B, Table S3). One logical outcome from these results is that excess CENP-C would encode a centromeric fiber that is less permissive to chromatin binding factors, such as the transcriptional machinery.

We tested this hypothesis by overexpressing CENP-C *in vivo* for three days, after which we purified kinetochore-associated CENP-A chromatin and kinetochore-depleted CENP-A chromatin by serial N-ChIP (Figure 3C). First, we assessed whether overexpression of CENP-C would also induce CENP-A chromatin compaction *in vivo*. We purified kinetochore-depleted CENP-A chromatin (second ACA N-ChIP) and measured compaction as above. We observed a doubling of compacted chromatin states relative to controls (Figure 3D, Table S3). Next, we measured the nucleosomal dimensions of the kinetochore-associated CENP-A nucleosomes, and of kinetochore-depleted CENP-A nucleosomes. In cells overexpressing CENP-C, CENP-A nucleosomes displayed a marked increase in particle height, whereas kinetochore-associated CENP-A nucleosomes did not display a change in particle height (2.0±0.5 nm vs 3.5±0.8 nm, and 2.7±1.0 nm vs 2.7±1.2 nm resp. Figure S5B, Table S4). These data suggest that in the CENP-C overexpression background, there is not only enhanced clustering and compaction of CENP-A chromatin, but also a general shift towards suppression of plasticity of individual CENP-A nucleosomes.

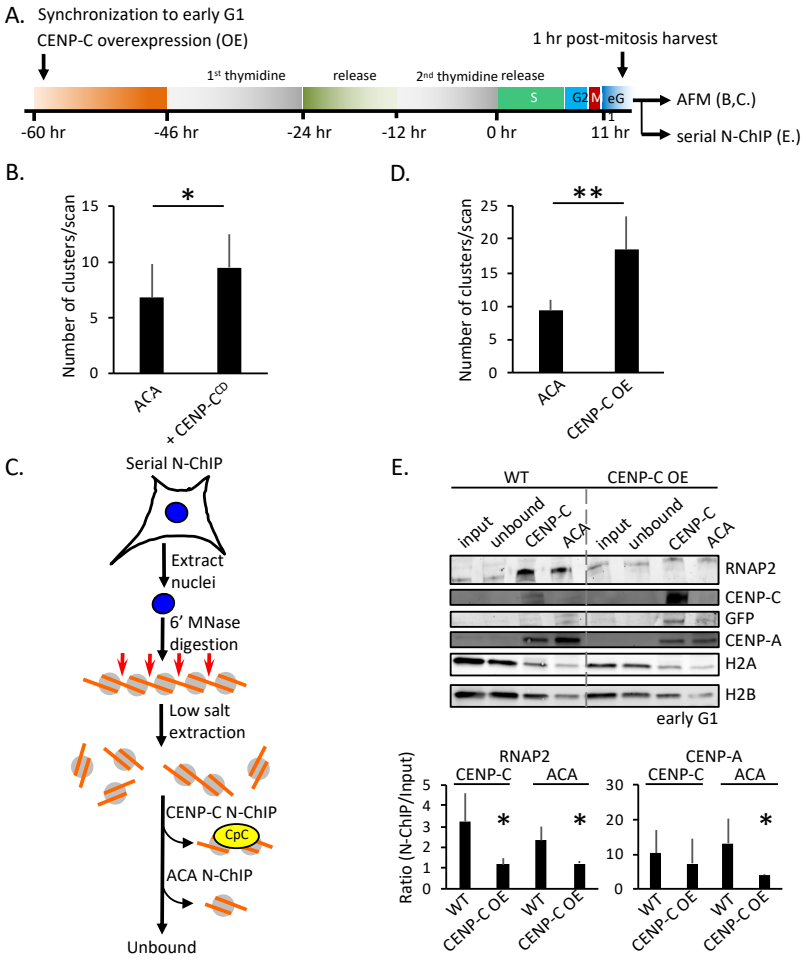

Figure 3. CENP-C overexpression compacts CENP-A chromatin, making it inaccessible to RNAP2

(A) Schematic representation how HeLa cells were synchronized to late M/early G1 by double thymidine block. (B) Chromatin compaction was measured by average circumference of particles, as this would distinguish both compacted chromatin and clustered nucleosomes from individual nucleosomes. *In vivo* ACA N-ChIP samples with and without either the addition of CENP-C^{CD}. (* p-value< 0.05) (C) Graphical representation of serial N-ChIP experimental procedure. (D) *In vivo* chromatin compaction was measured by average circumference of particles, as this would distinguish both compacted chromatin and clustered nucleosomes from individual nucleosomes. ACA N-ChIP samples with and without CENP-C overexpression (OE) were compared. (** p-value< 0.005) (E) Western blot analysis of serial N-ChIP probing for RNAP2 and various centromere and chromatin markers. Quantification of RNAP2 and CENP-A levels were determined (* p-value< 0.05).

CENP-C overexpression suppresses RNA polymerase 2 occupancy and *de novo* CENP-A loading

During late mitosis and early G1, RNAP2 is present at the centromere[43]. We wondered whether overexpression of CENP-C, and thus the induction of more compacted CENP-A chromatin, would lead to reduced accessibility for RNAP2. Indeed, by western blot analysis, when CENP-C is overexpressed we observed a significant reduction in RNAP2 at both CENP-A domains (3- and 2-fold reduction, resp.; t-test $p<0.05$; Figure 3D, Table S5).

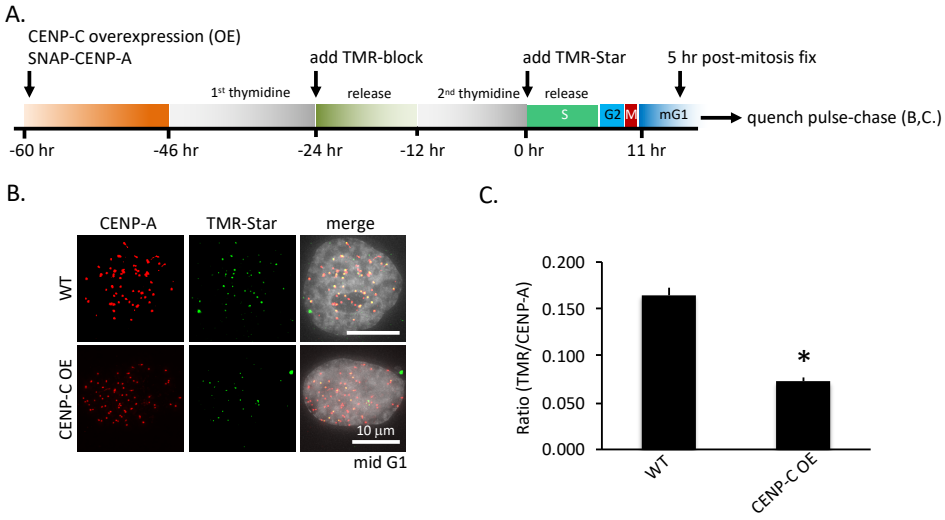

Figure 4. New CENP-A loading impaired upon CENP-C overexpression

(A) Schematic of experimental design. (B) *De novo* CENP-A incorporation was assessed by quench pulse-chase immunofluorescence. After old CENP-A was quenched with TMR-block, newly loaded CENP-A was stained with TMR-Star and foci intensity was measured over total CENP-A foci intensity. (C) Quantification of *de novo* CENP-A loading (** p-value< 0.005).

Work from several labs have recently suggested that transcription of centromeric DNA is required for *de novo* CENP-A loading[43]. In this scenario, overexpression of CENP-C, which suppressed RNAP2 at centromeres (Figure 3E), should also lead to reduced *de novo* CENP-A loading. An initial clue leading to this possibility was already gleaned from our initial western

blot analysis, in which overexpression of CENP-C led to a significant reduction in the kinetochore-depleted CENP-A population (t-test $p<0.05$; Figure 3E, Table S5). We wanted test the idea that this reduction in CENP-A levels might have arisen from reduced *de novo* CENP-A loading. Therefore, we turned to the well-established SNAP-tagged CENP-A system combined with quench pulse-chase immunofluorescence[27] to track *de novo* integrated CENP-A. Strikingly, in the CENP-C overexpression background, we observed a 2.3-fold reduction of *de novo* incorporation of CENP-A (t-test $p<0.01$; Figure 4, Table S6).

Taken together, these data suggest elastic CENP-A nucleosomes create an intrinsically open chromatin environment, which is rigidified by CENP-C.

Discussion

Previous computational modeling experiments suggested that nucleosomes containing the CENP-A can intrinsically sample altered conformations and are structurally "frustrated" compared to canonical H3 nucleosomes[31]. In a plasticine vs. rock model, we predicted that a structurally "frustrated" nucleosome would manifest itself in distinctly different elasticity. Indeed, by novel single molecule nano-indentation force spectroscopy, CENP-A nucleosomes are twice as elastic as canonical nucleosomes (Figure 1).

FRET experiments of *in vitro* reconstituted CENP-A mononucleosomes showed restricted DNA gyre gapping and sliding[33]. These data suggested that kinetochore components could choose and fix one or a few specific conformational states. Indeed, when we modeled CENP-A nucleosomes alone, vs. those bound to CENP-C^{CD}, we observed both, a marked diminution of motion, and free

energy minima, representing lost conformational flexibility (Figure 2A,B, S1, S2). The diminution of conformational flexibility correlates with a loss of elasticity of CENP-A nucleosomes upon CENP-C^{CD} binding (Figure 2D,E).

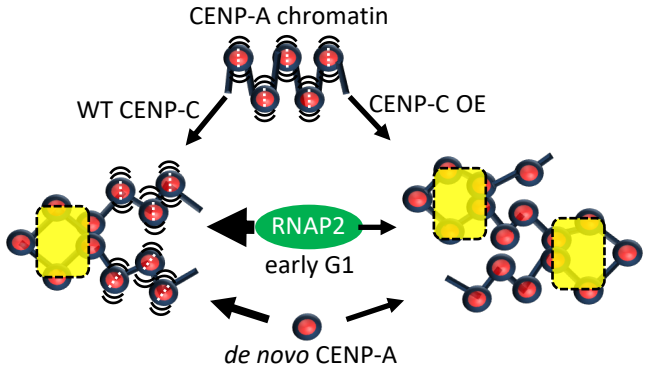

Figure 5. A balance between elastic and rigidified CENP-A nucleosomes governs centromere chromatin fidelity

Working model showing that a balance exists between the intrinsically elastic CENP-A nucleosomes and its kinetochore-induced rigidified form. The elastic CENP-A chromatin creates an open chromatin state permissive of the recruitment of the transcriptional machinery, which is critical for *de novo* incorporation of CENP-A. When this balance is disturbed by for instance CENP-C overexpression, CENP-A chromatin becomes overcompacted, which impedes the necessary recruitment of the transcriptional machinery, and subsequently reduced new CENP-A loading.

Our hypothesis is that elasticity of CENP-A contributes to the accessibility of the centromeric chromatin fiber, potentially by allowing nucleosomes to deform or slide more easily. Indeed, in support of this idea, overexpression of CENP-C resulted in centromere chromatin compaction and decreased localization of RNAP2 at CENP-A chromatin, which correlates with the loss of *de novo* CENP-A loading (Figure 3, 4). In a working model based on these data, a balance between kinetochore bound rigid CENP-A nucleosomes, and unbound elastic CENP-A nucleosomes

exists to maintain the fidelity of centromere chromatin. In this working model, intrinsically open chromatin state is created by CENP-A nucleosomes are potentially bound to other factors (such as Mis18BP1), permitting recruitment of RNAP2, which in turn facilitates incorporation of new CENP-A nucleosomes (Figure 5). When this balance is disturbed resulting in loss of unbound CENP-A chromatin, for instance through overexpression of CENP-C, the level of centromeric CENP-A will reduce, jeopardizing centromeric fidelity. This working model, we think, also sheds light on the paradox of how centromeric transcription required for new CENP-A loading is enabled in the context of actively engaged kinetochores.

Not all nucleosomes are identical, as many contain histone variants, giving them distinct functions. In this report, we demonstrate how a single histone variant can alter the intrinsic biophysical properties of a nucleosome, which can be over-ridden by its cognate protein partners, thereby impacting the structural and functional state of the resulting chromatin fiber. An ongoing extension of this work is to test whether partnering with alternative histone variants, such as that reported in cancer cells[41,43-46], impacts CENP-A nucleosomal elasticity. In this context, testing whether suppressing such cancer-specific partnerships changes the outcome at ectopically occupied loci, most significantly, at neocentromere like domains[41,46] is an outstanding avenue of future investigation.

We note that centromeric DNA and centromeric protein genes are rapidly evolving[12-17,47]. Not all species share all kinetochore components: centromeric genes are lost, duplicated, and sometimes invented[48-50]. Despite these evolutionary changes, the distinctive chromatin structure of centromeres must be maintained, to accomplish its conserved function during mitosis.

Investigating whether CENP-A structures and their elasticities are conserved, or co-evolve with specific kinetochore proteins, will also provide critical clues into what drives the evolution of centromere chromatin, in turn serving as an excellent model for studying the evolution of epigenetic systems in the genome.

Authors contribution

Conceptualization: D.P.M. and Y.D.; Methodology: D.P.M., T.R., M.P., M.B., and Y.D.; Investigation: D.P.M., T.R., M.P., M.B., and S.A.G.; Writing – original draft: D.P.M. and Y.D.; Writing – Review & Editing: D.P.M., T.R., G.A.P., and Y.D.; Funding Acquisition: S.A.G., G.A.P., and Y.D.; Visualization: D.P.M; Supervision: Y.D.

Acknowledgements

We thank Tom Misteli, Sam John, and members of our laboratory for critical comments; Will Heinz and Emilios Dimitriadis for discussions on force spectroscopy experiments; Stephan Diekmann and Dan Foltz for gifting GFP-CENP-C and SNAP-tagged CENP-A constructs, respectively. DPM, TR, MB, DS, and YD are supported by the Intramural Research Program of the Center for Cancer Research at the National Cancer Institute/NIH. MP is supported by the joint NCI-UMD Cancer Technology Partnership. GAP is supported by NSF grant CHE-1363081.

References

1. Peterson, C.L. & Almouzni, G., 2013, Nucleosome dynamics as modular systems that integrate DNA damage and repair, *Cold Spring Harb Perspect Biol*, 5(9), pp. a012658.

2. Yadav, T., Quivy, J.P., & Almounzi, G., 2018, Chromatin plasticity: a versatile landscape that underlies cell fate and identity, *Science*, 361(6409:, pp. 1332-6.
3. Bellush, J.M., & Whitehouse, I., 2017, DNA replication through a chromatin environment, *Philos Trans R Soc Lond B Biol Sci*, 372(1731), pp. 20160287
4. Petryk, N., Dalby, M., Wenger, A., Stromme, C.B., Strandsby, A., Andersson, R., & Groth, A., 2018, MCM2 promoters symmetric inheritance of modified histones during DNA replication. *Science*, 361(6409), pp. 1388-92.
5. Weber, C.M., & Henikoff, S., 2014, Histone variants: dynamic punctuation in transcription, *Genes Dev*, 28(7), pp. 672-82.
6. Rothbart, S.B., & Strahl, B.D., 2009, Interpreting the language of histone and DNA modifications. *Biochim Biophys Acta*, 1839(8), pp. 627-43.
7. Luger, K., Dechassa, M.L., & Tremethick, D.J., 2012, New insights into nucleosome and chromatin structure: an ordered state or a disordered affair? *Nat Rev Mol Cell Biol*, 13(7), pp. 436-47.
8. Bowman, G.D. & Poirier, M.G., 2015, Post-translational modifications of histones that influence nucleosome dynamics, *Chem Rev*, 115(6), pp. 2274-95.
9. Palozola, K.C., Liu, H., Nicetto, D., & Zaret, K.S., 2018, Low-level, global transcription during mitosis and dynamic gene reactivation during mitotic exit, *Cold Spring Harb Symp Quant Biol*, 82, pp. 197-205.
10. Ginno, P.A., Burger, L., Seebacher, J., Iesmantavicius, V., & Schübeler, D., 2018, Cell cycle-resolved chromatin proteomics reveals the extent of mitotic preservation of the genomic regulatory landscape. *Nat Commun*, 9(1), pp. 4048.

11. Bloom, K.S., 2008, Beyond the code: the mechanical properties of DNA as they relate to mitosis, *Chromosoma*, 117(2):103-10.
12. Cooper, J.L. & Henikoff, S., 2004, Adaptive evolution of the histone fold domain in centromeric histones, *Mol Biol Evol*, 21(9), pp. 1712-8.
13. Malik, H.S. & Henikoff, S., 2001, Adaptive evolution of Cid, a centromere-specific histone in Drosophila, *Genetics*, 157(3), pp. 1293-8.
14. Talbert, P.B., Bryson, T.D. & Henikoff, S., 2004, Adaptive evolution of centromere proteins in plants and animals, *J Biol*, 3(4), p. 18.
15. Meraldi, P., McAinsh, A.D., Rheinbay, E. & Sorger, P.K., 2006, Phylogenetic and structural analysis of centromeric DNA and kinetochore proteins, *Genome Biol*, 7(3), p. R23.
16. Maheshwari, S., Tan, E.H., West, A., Franklin, F.C., Comai, L. & Chan, S.W., 2015, Naturally occurring differences in CENH3 affect chromosome segregation in zygotic mitosis of hybrids, *PLoS Genet*, 11(1), p. e1004970.
17. Melters, D.P., Bradnam, K.R., Young, H.A., Telis, N., May, M.R., Ruby, J.G., Sebra, R., Peluso, P., Eid, J., Rank, D., et al, 2013, Comparative analysis of tandem repeats from hundreds of species reveals unique insights into centromere evolution, *Genome Biol*, 14(1), p. R10.
18. Régnier, V., Vagnarelli, P., Fukagawa, T., Zerjal, T., Burns, E., Trouche, D., Earnshaw, W. & Brown, W., 2005, CENP-A is required for accurate chromosome segregation and sustained kinetochore association of BubR1, *Mol Cell Biol*, 25(10), pp. 3967-81.
19. Carroll, C.W., Milks, K.J. & Straight, A.F., 2010, Dual recognition of CENP-A nucleosomes is required for centromere assembly, *J Cell Biol*, 189(7), pp. 1143-55.

20. Mendiburo, M.J., Padeken, J., Fülöp, S., Schepers, A. & Heun, P., 2011, Drosophila CENH3 is sufficient for centromere formation, *Science*, 334(6056), pp. 686-90.
21. Pesenti, M.E., Weir, J.R. & Musacchio, A., 2016, Progress in the structural and functional characterization of kinetochores, *Curr Opin Struct Biol*, 37, pp. 152-63.
22. Fukagawa, T., Pendon, C., Morris, J. & Brown, W., 1999, CENP-C is necessary but not sufficient to induce formation of a functional centromere, *The EMBO journal*, 18(15), pp. 4196-209.
23. McKinley, K.L. & Cheeseman, I.M., 2016, The molecular basis for centromere identity and function, *Nat Rev Mol Cell Biol*, 17(1), pp. 16-29.
24. Kalitsis, P., Fowler, K.J., Earle, E., Hill, J. & Choo, K.H., 1998, Targeted disruption of mouse centromere protein C gene leads to mitotic disarray and early embryo death, *Proc Natl Acad Sci U S A*, 95(3), pp. 1136-41.
25. Howman, E.V., Fowler, K.J., Newson, A.J., Redward, S., MacDonald, A.C., Kalitsis, P. & Choo, K.H., 2000, Early disruption of centromeric chromatin organization in centromere protein A (Cenpa) null mice, *Proc Natl Acad Sci U S A*, 97(3), pp. 1148-53.
26. Suzuki, A., Hori, T., Nishino, T., Usukura, J., Miyagi, A., Morikawa, K. & Fukagawa, T., 2011, Spindle microtubules generate tension-dependent changes in the distribution of inner kinetochore proteins, *J Cell Biol*, 193(1), pp. 125-40.
27. Bodor, D.L., Valente, L.P., Mata, J.F., Black, B.E. & Jansen, L.E., 2013, Assembly in G1 phase and long-term stability are unique intrinsic features of CENP-A nucleosomes, *Mol Biol Cell*, 24(7), pp. 923-32.

28. Smoak, E.M., Stein, P., Schultz, R.M., Lampson, M.A. & Black, B.E., 2016, Long-Term Retention of CENP-A Nucleosomes in Mammalian Oocytes Underpins Transgenerational Inheritance of Centromere Identity, *Curr Biol*, 26(8), pp. 1110-6.

29. Foltz, D.R., Jansen, L.E., Balley, A.O., Yates, Jr 3rd, J.R., Bassett, E.A., Wood, S., Black, B.E., & Cleveland, D.W., 2009, Centromere-specific assembly of CENP-A nucleosomes is mediated by HJURP. *Cell*, 137(3), pp. 472-84.

30. Dunleavy, E.M., Roche, D., Tagami, H., Lacoste, N., Ray-Gallet, D., Nakamura., Y., Daigo., Y., Nakatani, Y., & Almouzni-Pettinotti, G., 2009, HJURP is a cell-cycle-dependent maintenance and deposition factor of CENP-A at centromeres. *Cell*, 137(3), pp. 485-97.

31. Winogradoff, D., Zhao, H., Dalal, Y. & Papoian, G.A., 2015, Shearing of the CENP-A dimerization interface mediates plasticity in the octameric centromeric nucleosome, *Sci Rep*, 5, p. 17038.

32. Vinckier, A., & Semenza, G., 1998, Measuring elasticity of biological materials by atomic force miscroscopy. *FEBS Lett*, 430, pp. 12-6.

33. Rakshit, T., Banerjee, S., Mishra, S., Mukhopadhyay, R., 2013, Nanoscale mechano-electronic behavior of a metalloprotein as a variable of metal content. *Langmuir*, 29(40):12511-9.

34. Roos, W.H., 2018, AFM nanoidentation of protein shells, expanding the approach beyond viruses. *Semin Cell Dev Biol*, 73, pp. 145-152.

35. Heinz, W.F., & Hoh, J.H., Spatially resolved force spectroscopy of biological surfaces using the atomic force microscope. *Trends Biotechnol.* 17(4):143-50 .

36. Butt, H.-J., Cappella, B., & Kappl, M., 2005, Force measurements with the atomic force microscope: technique, interpretation and application, *Surface Sci Rep*, 59:1-152.

37. Walkiewicz, M. P., Dimitriadis, E. K. & Dalal, Y., 2014, CENP-A octamers do not confer a reduction in nucleosome height by AFM, *Nat Struct Mol Biol,* 21, pp. 2-3

38. Athwal, R.K., Walkiewicz, M.P., Baek, S., Fu, S., Bui, M., Camps, J., Ried, T., Sung, M.H. & Dalal, Y., 2015, CENP-A nucleosomes localize to transcription factor hotspots and subtelomeric sites in human cancer cells, *Epigenetics Chromatin*, 8, p. 2.

39. Falk, S.J., Guo, L.Y., Sekulic, N., Smoak, E.M., Mani, T., Logsdon, G.A., Gupta, K., Jansen, L.E., Van Duyne, G.D., Vinogradov, et al, 2015, Chromosomes. CENP-C reshapes and stabilizes CENP-A nucleosomes at the centromere, *Science*, 348(6235), pp. 699-703.

40. Falk, S.J., Lee, J., Sekulic, N., Sennett, M.A., Lee, T.H. & Black, B.E., 2016, CENP-C directs a structural transition of CENP-A nucleosomes mainly through sliding of DNA gyres, *Nat Struct Mol Biol*, 23(3), pp. 204-8.

41. Guo, L.Y., Allu, P.K., Zandarashvili, L., McKinley, K.L., Sekulic, N., Dawicki-McKenna, J.M., Fachinetti, D., Logsdon, G.A., Jamiolkowski, R.M., Cleveland, D.W., et al, 2017, Centromeres are maintained by fastening CENP-A to DNA and directing an arginine anchor-dependent nucleosome transition, *Nat Commun*, 8, p. 15775.

42. Roulland, Y., Ouararhni, K., Naidenov, M., Ramos, L., Shuaib, M., Syed, S.H., Lone, I.N., Boopathi, R., Fontaine, E., Papai, G., et al, 2016, The Flexible Ends of CENP-A Nucleosome Are Required for Mitotic Fidelity, *Mol Cell*, 63(4), pp. 674-85.

43. Müller, S., & Almouzni, G., 2017, Chromatin dynamics during the cell cycle at centromeres, *Nat Rev Genet*, 18(3):192-206.

44. Lacoste, N., Woolfe, A., Tachiwana, H., Garea, A.V., Barth, T., Cantaloube, S., Kurumizaka, H., Imhof, A. & Almouzni, G., 2014, Mislocalization of the centromeric histone variant CenH3/CENP-A in human cells depends on the chaperone DAXX, *Mol Cell*, 53(4), pp. 631-44.

45. Fang, J., Liu, Y., Wei, Y., Deng, W., Yu, Z., Huang, L., Teng, Y., Yao, T., You, Q., Ruan, H., et al, 2015, Structural transition of centromeric chromatin regulate the cell cycle-dependent recruitment of CENP-N, *Genes Dev*, 29(10):1058-73.

46. Nye, J., Sturgill, D., Athwal, R.K., & Dalal, Y., 2018, HJURP antagonizes CENP-A mislocalization driven by the H3.3 chaperones HIRA and DAXX, *PLoS ONE*, *in press*.

47. Henikoff, S., Ahmad, K. & Malik, H.S., 2001, The centromere paradox: stable inheritance with rapidly evolving DNA, *Science*, 293(5532), pp. 1098-102.

48. Ross, B.D., Rosin, L., Thomae, A.W., Hiatt, M.A., Vermaak, D., de la Cruz, A.F., Imhof, A., Mellone, B.G. & Malik, H.S., 2013, Stepwise evolution of essential centromere function in a Drosophila neogene, *Science*, 340(6137), pp. 1211-4.

49. Drinnenberg, I.A., Henikoff, S. & Malik, H.S., 2016, Evolutionary Turnover of Kinetochore Proteins: A Ship of Theseus? *Trends Cell Biol*, 26(7), pp. 498-510.

50. van Hooff, J.J., Tromer, E., van Wijk, L.M., Snel, B. & Kops, G.J., 2017, Evolutionary dynamics of the kinetochore network in eukaryotes as revealed by comparative genomics, *EMBO Rep*.

Online Me**thods**

Key Resources Table

Reagents or Resource	**Source**	**Identifier**
Antibodies		
ACA serum	BBI Solutions	SG140-2
Anti-GFP	Santa Cruz	sc-9996
Anti-CENP-A (mouse)	Abcam	ab13939
Anti-CENP-A (rabbit)	Abcam	ab45694
Anti-CENP-A (rabbit)	Milipore	04-205
Anti-CENP-B (rabbit)	Santa Cruz	sc-22788
Anti-CENP-C (guinea pig)	MBL Int.	PD030
Anti-CENP-C (rabbit)	Santa Cruz	sc-22789
Anti-RNA polymerase II	Millipore	05-623
Anti-RNA polymerase II	Abcam	ab5095
Anti-CENP-N	Avivasysbio	ARP57258-P050
Anti-CENP-I	Bethyl	A303-374A
Anti-CENP-T	Bethyl	A302-314A
Anti-CENP-W	Invitrogen	PA5-34441
Anti-MIS12	Abcam	ab70843
Anti-HEC1/NDC80	GeneTex	GTX70268
Anti-macroH2A.1	Abcam	ab37264
Anti-γH2A.X	Abcam	ab2893
Anti-γH2A.X	Abcam	ab11174
Anti-H2A.Z	Abcam	ab4179
Anti-H2A	Abcam	ab18255
Anti-H2B	Abcam	ab1790
Anti-H4	Cell Signaling	2935T
Anti-H3	Santa Cruz	sc-8654
Software and Algorithms		
RepBase		hhtp://www.girinst.org/repbase
Gwyddion		http://gwyddion.net/
R		https://www.r-project.org/
NIH ImageJ		https://imagej.nih.gov/ij/
Bio-Formats		https://www.openmicroscopy.org/bio-formats/
PyMOL		https://pymol.org/2/

CRaQ		http://facilities.igc.gulbenkian.pt/microscopy/microscopy-macros.php

Contact for Reagent and Resource Sharing

Requests for further information or reagents should be directed to the Lead Contact, Yamini Dalal (dalaly@mail.nih.gov)

Experimental Model and Subject Detail

HeLa cells (female cells derived from cervical adenocarcinoma) were obtained from ATCC CCL-2 and grown at 37ºC and 5% CO2 in T-175 tissue culture flasks from Sarstedt (Cat. #83.3912.002).

Methods Details

All-atom computational modeling

Two nucleosomal systems were built for simulation: the CENP-A nucleosome as described previously[1] and the CENP-A nucleosome with CENP-C fragment bound from PDB ID: 4X23[2]. The CENP-C^{CD} fragments were docked onto the CENP-A interface using the CE algorithm[3] of PyMOL (The PyMol Molecular Graphics System). Both systems were started from the final time point of our previous 1 μs simulation and the coordinates, velocities, parameters, and system setup and analysis methods were replicated[1]. Both CENP-A and CENP-A with one and two CENP-C^{CD} bound were simulated for an additional microsecond and the first 600 ns of simulation time were truncated from the dataset for further analysis and to account for equilibration. Furthermore, we calculated the relative positions of three phosphate backbone

atoms at positions -33, -43, and +38 numbered from the 5' (−) to 3' (+) direction relative to the pseudo-dyad. The distances between these points and the skew of the triangle formed were measured and then plotted with the initial position of residue -33 set to (0,0) on an xy-plane. The distribution of Δy and Δx of +38 relative to -33 and -34 was used to measure DNA gaping and sliding respectively. These distributions were visualized with standard box plots showing the mean, the central rectangle showing the interquartile range, and whiskers extending to the extrema. The distribution of polygons contains the minima and maxima of all three vertices were plotted visually with triangles to visually represent changes in skew and the range of sizes.

Native Chromatin-Immunoprecipitation and western blotting

Human cell line HeLa were grown in DMEM (Invitrogen/ThermoFisher Cat #11965) supplemented with 10% FBS and 1X penicillin and streptomycin cocktail. N-ChIP experiments were performed without fixation. After cells were grown to ~80% confluency, they were harvested as described here[1,4], but with a few modifications. In short, cells were harvested, washed with PBS and PBS containing 0.1% Tween 20 (Sigma-Aldrich cat #P7949). Nuclei were released with TM2 (20 mM Tris-HCl, pH 8.0; 2 mM $MgCl_2$; 0.5 mM PMSF) with 0.5% Nonidet P-40 (Sigma-Aldrich cat #74385). Afterwards, nuclei were washed with TM2 and dissolved in a total volume of 2 mL of 0.1 M TE (10 mM Tris-HCl, pH 8.0; 0.2 mM EDTA, 100 mM NaCl). Subsequently, chromatin was digested for 6 minutes with 0.25 U MNase (Sigma-Aldrich cat #N3755-500UN) and supplemented with 1.5 mM $CaCl_2$. MNase reaction was quenched with 10 mM EGTA. All centrifugations were done at 1000 rpm at 4ºC. The cell or nuclei pellet was only tapped once to facilitate braking them up. Supernatant was removed, and chromatin extracted

overnight in low salt solution (0.5X PBS; 0.1 mM EGTA supplemented with a protease inhibitor cocktail (Roche cat #05056489001). N-ChIP chromatin bound to Protein G Sepharose beads (GE Healthcare cat #17-0618-02) were washed twice with ice cold 0.5X PBS and spun down for 1 minute at 4ºC at 800 rpm. For a serial N-ChIP, the first unbound fraction was saved and subjected to a second N-ChIP. Westerns were done using LiCor's Odyssey CLx scanner and Image Studio v2.0.

For CENP-C overexpression we transfected HeLa cells with pEGFP-CENP-C using the Amaxa Cell Line Nucleofector Kit R (Lonza cat#VVCA-1001) per manufacturer's instructions. HeLa cells were synchronized to early G1 by double thymidine block (0.5 mM, Sigma-Aldrich cat#T9250). After the first block of 22 hours, cells were released for 12 hours, followed by a second thymidine block of 12 hours. Cells were released for approximately 11 hours, which corresponds to early G1, based on our previous reports[1,4,5].

AFM and image analysis

Imaging of CENP-C and CENP-A N-ChIP and bulk chromatin was performed as described[6,7] with the following modifications. Imaging was performed by using standard AFM equipment (Oxford Instruments, Asylum Research's Cypher S AFM, Santa Barbara, CA) with silicon cantilevers (OTESPA or OTESPA-R3 with nominal resonances of ~300 kHz, stiffness of ~42 N/m, and tip radii of 3–7 nm and FESP with ~75 kHz, 2.8 N/m and 7 nm, respectively, Bruker-Nano) in noncontact tapping mode. Usually, 10 µl stock solution of 4× diluted CENP-C or 10× diluted CENP-A chromatin or 1,000× diluted bulk chromatin was deposited on APS-mica. APS-mica was prepared as previously described[6,7]. The samples were incubated for 10 min, rinsed

gently to remove salts, and dried under vacuum before imaging. Images were acquired at high resolution and preprocessed on the NanoScope instrument software.

For the compaction study, we added 1 ng CENP-C^{CD} to purified ACA samples and incubated them for 30 minutes prior to deposition on APS-mica and subsequent imaging. To determine the compaction frequency, we manually counted compacted chromatin clusters based on their size being at least twice as wide as an individual nucleosome, but with an identifiable entry and exit DNA strand.

Automated image analysis was performed as described in [6] by using Gwyddion software, NIH ImageJ software (NIH), and R software (instead of Microsoft Excel). A total of six biological replicates were performed for CENP-C experiments and three biological replicates for the CENP-A and bulk chromatin experiments. Bulk chromatin from the same preparation was imaged in parallel to get the baseline octameric range. For all samples, manual spot analyses were performed to confirm accuracy of automated analyses.

Force spectroscopy

In vitro reconstitution of CENP-A (CENP-A/H4 cat#16-010 and H2A/H2B cat#15-0311, EpiCypher, Research Triangle Park, NC) and H3 (H3/H4 cat#16-0008 and H2A/H2B cat#15-0311, EpiCypher Research Triangle Park, NC) nucleosomes were performed as previously described[6,7] CENP-$C_{482-527}$ fragment (ABI Scientific, Sterling, VA) was added in 2.2-fold molar excess to CENP-A nucleosomes. To be able to measure the Young's modulus, the reconstituted chromatin was kept in solution containing 67.5 mM NaCl and 2 mM Mg^{2+} and a different

cantilever (Olympus micro cantilever cat# BL-AC40TS-C2. Before each experiment, the spring constant of each cantilever was calibrated using both GetReal™ Automated Probe Calibration of Cypher S and the thermal noise method[8]. Obtained values were in the order of 0.1 N/m. As a reference to obtain the indentation values, the photodiode sensitivity was calibrated by obtaining a force curve of a freshly cleaved mica surface. All experiments were conducted at room temperature. Force-curves for ~50 nucleosomes for all three conditions were measured using both 'Pick a Point' and force-mapping mode. The maximum indentation depth was limited to ~1.5 nm and the maximum applied force was 150-200 pN. For our analyses, we used Hertz model with spherical indenter geometry for Young's Modulus measurements, $\delta = [3(1 - \nu^2)/(4ER^{1/2})]^{2/3}F^{2/3}$ (for a spherical indenter), where ν is the Poisson ratio of the sample, which is assumed to be 1/3 as in studies reported previously[9,10]; δ, F, E, and R are the indentation, force, Young's modulus of the sample and radius of the tip respectively. The radius of the tip was confirmed by SEM and found to be about 10 nm in width.

Immunostaining of mitotic chromosomes

HeLa cells were synchronized to mitosis with double thymidine block. Primary antibodies CENP-C and CENP-A were used at dilution 1:1000. Alexa secondary (488, and 568) were used at dilution of 1:1000. Images were obtained using DeltaVision RT system fitted with a CoolSnap charged-coupled device camera and mounted on an Olympus IX70. Deconvolved IF images were processed using ImageJ. Mitotic defects (lagging chromosomes and/or multipolar spindles) were counted for 83 and 76 cells (mock, GFP-CENP-C, respectively).

Quench pulse-chase immunofluorescence

To quantify *de novo* assembled CENP-A particles, we transfected HeLa cells with SNAP-tagged CENP-A (generous gift from Dan Foltz) in combination with either empty vector or GFP-CENP-C using the Amaxa Nucleofector kit R (Lonza Bioscience, Walkersville, MD) per instructions. The quench pulse-chase experiment was performed according to Bodor et al 2012. In short, following transfection, cells were synchronized with double thymidine block. At the first release TMR-block (S9106S, New England Biolabs, Ipswich, MA) was added per manufactures instruction and incubated for 30 min at 37ºC, followed by three washes with cell culture media. At the second release TMR-Star (S9105S, New England Biolabs, Ipswich, MA) was added per manufactures instructions and incubated for 15 min at 37ºC, followed by three washes with cell culture media. Fourteen hours after adding TMR-Star, cells were fixed with 1% paraformaldehyde in PEM (80 mM K-PIPES pH 6.8, 5 mM EGTA pH 7.0, 2 mM $MgCl_2$) for 10 min at RT. Next, cells were washed the cells three times with ice cold PEM. To extract soluble proteins, cells were incubated with 0.5% Triton-X in CSK (10 mM K-PIPES pH 6.8, 100 mM NaCl, 300 mM sucrose, 3 mM $MgCl_2$, 1 mM EGTA) for 5 min at 4ºC. The cells were rinsed with PEM and fixed for a second time with 4% PFA in PEM for 20 min at 4ºC. Next, the cells were washed three times with PEM. Cells were permeabilized with 0.5% Triton-X in PEM for 5 min at RT and subsequently washes three times with PEM. Next, the cells were incubated in blocking solution (1X PBS, 3% BSA, 5% normal goat serum) for 1 hr at 4ºC. CENP-A antibody (ab13979 1:1000) was added for 1 hr at 4ºC, followed by three washes with 1X PBS-T. Anti-mouse secondary (Alexa-488 1:1000) was added for 1hr at 4ºC, followed by three 1X PBS-T and two 1X PBS washes. Following air-drying, cells were mounted with Vectashield with DAPI (H-1200, Vector Laboratories, Burlingame, CA) and the coverslips were sealed with nail polish. Images were collected using a DeltaVision RT system fitted with a CoolSnap charged-coupled

device camera and mounted on an Olympus IX70. Deconvolved IF images were processed using ImageJ and the macro CRaQ[11].

Quantification and Statistical Analyses

Significant differences for nucleosome height measurement from AFM analyses and significant differences for immunostaining quantification, and chromatin compaction quantification, were performed using the t-test as described in the figure legends and main text. Significant differences for the Young's modulus of *in vitro* reconstituted H3, CENP-A, and CENP-A + CENP-C^{CD} were determined using 1-way ANOVA test. Significance was determined at $p < 0.05$.

References

1. Bui, M., Pitman, M., Nuccio, A., Roque, S., Donlin-Asp, P.G., Nita-Lazar, A., Papoian, G.A. & Dalal, Y., 2017, Internal modifications in the CENP-A nucleosome modulate centromeric dynamics, *Epigenetics Chromatin*, 10, p. 17.
2. Kato, H., Jiang, J., Zhou, B.R., Rozendaal, M., Feng, H., Ghirlando, R., Xiao, T.S., Straight, A.F. & Bai, Y., 2013, A conserved mechanism for centromeric nucleosome recognition by centromere protein CENP-C, *Science*, 340(6136), pp. 1110-3.
3. Shundyalov, I.N., & Bourne, P.E., 1998, Protein structure alignment by incremental combinatorial extension (CE) of the optimal path. *Protein Eng*, 11(9), pp. 739-47.
4. Bui, M., Dimitriadis, E.K., Hoischen, C., An, E., Quénet, D., Giebe, S., Nita-Lazar, A., Diekmann, S. & Dalal, Y., 2012, Cell-cycle-dependent structural transitions in the human CENP-A nucleosome in vivo, *Cell*, 150(2), pp. 317-26.

5. Quénet, D., & Dalal, Y., 2014, A long non-coding RNA is required for targeting centromeric protein A to the human centromere, *eLife*, 3:e03254.
6. Walkiewicz, M. P., Dimitriadis, E. K. & Dalal, Y., 2014, CENP-A octamers do not confer a reduction in nucleosome height by AFM, *Nat Struct Mol Biol,* 21, pp. 2-3.
7. Dimitriadis, E.K., Weber, C., Gill, R.K., Diekmann, S., & Dalal Y., 2010, Tetrameric organization of vertebrate centromeric nucleosomes. *Proc Natl Acad Sci USA,* 107(47), pp. 20317-22.
8. Hutter, J.L., & Beckhoefer, J., 1993, Calibration of atomic-force microscope tips, *Rev Sci Instrum*, 64(7):1868-73.
9. Radmacher, M., Fitz, M., Cleveland, J.P., Walters, D.A., & Hansma, P.K., 1994, Imaging adhesion forces and elasticity of lysozyme adsorbed on mica with the atomic force microscope, *Langmuir*, 10(10):3809-14.
10. Rakshit, T., Banerjee, S., Mishra, S., Mukhopadhyay, R., 2013, Nanoscale mechano-electronic behavior of a metalloprotein as a variable of metal content. *Langmuir*, 29(40):12511-9.
11. Bodor, D.L., Rodriguez, M.G., Moreno, N., & Jansen, L.E., 2012, Analysis of protein turnover by quantitative SNAP-based pulse-chase imaging, *Curr Protoc Cell Biol*, Chapter 8, Unit 8.

Supplemental Figure Legends

Figure S1. CENP-A nucleosomes display diminished local flexibility when bound to CENP-C^{CD}

(A) The distance between the center of mass (COM) of histone dimers is shown in blue for CENP-A + CENP-C^{CD} and in red for CENP-A. Upon CENP-C^{CD} binding the center of mass of various histone dimer pairs of the CENP-C nucleosome is limited, which means that CENP-C^{CD} induces a global loss of CENP- A nucleosome flexibility. (B) Residue root mean square fluctuations (RMSF) shows freezing of local flexibility in the CENP-A nucleosome shown in red and with CENP-C^{CD} bound shown in blue. In the region of CENP-C^{CD} binding, the first heterotypic half on the top panel, CENP-C^{CD} is seen to freeze the acidic patch and the loop 1 region of CENP-A. Dashed lines separate individual histones.

Figure S2. Two CENP-C^{CD} fragment strengthens rigidification of CENP-A nucleosomes

(A) The distance between the center of mass (COM) of histone dimers is shown in red for CENP-A, blue for CENP-A + 1 CENP-C^{CD}, and in orang for CENP-A + 2 CENP-C^{CD}. Two CENP-C^{CD} fragment exaggerated the COM distances compared to a single CENP-C^{CD} fragment, which means that 2 CENP-C^{CD} further induces a global loss of CENP-A nucleosome flexibility. (B) Residue root mean square fluctuations (RMSF) shows freezing of local flexibility in the CENP-A nucleosome shown in red, 1 CENP-C^{CD} bound shown in blue, and 2 CENP-C^{CD} bound shown in orange. In the region of CENP-C^{CD} binding, the first heterotypic half on the top panel, CENP-C is seen to freeze the acidic patch and the loop 1 region of CENP-A. One CENP-C^{CD} creates asymmetry, especially at the C-terminal end of H2A and H2B, this is abrogated when the second CENP-C^{CD} is bound. Dashed lines separate individual histones. (C) All-atom computational modeling of DNA gyre separation or DNA gyre sliding of CENP-A nucleosome

alone or bound to either 1 or 2 CENP-C^{CD} fragments. In each panel, each triangle represents a snapshot from simulation.

Figure S3. CENP-C overexpression leads to increased mitotic defects

Quantification of mitotic defects (multipolar spindles and/or lagging chromosomes) in HeLa cells with or without three days of CENP-C overexpression.

Figure S4. CENP-C overexpression did not increase double strand DNA breaks

Representative images of either wild-type or CENP-C overexpressing HeLa cells. HeLa cells were transfected 3 days and synchronized to early G1 prior to fixation and staining for CENP-C, CENP-A, and γH2A.X, a dsDNA break marker. No difference in γH2A.X foci was observed between the two samples.

Figure S5. Chromatin compaction was altered upon exposure to CENP-C, but CENP-C associated CENP-A nucleosomes remained unchanged.

(A) Representative images of either *in vitro* reconstituted CENP-A nucleosomes with or without CENP-C^{CD}, or *in vivo* extracted ACA N-ChIP from either untreated sample where we added 1 ng CENP-C^{CD}, or WT versus CENP-C OE. (B) Quantification of nucleosomal particle heights of both elastic (ACA N-ChIP) and rigidified (CENP-C N-ChIP) CENP-A nucleosomes (unbound and bound CENP-A's) in wild-type or CENP-C overexpressing cells in early G1.

Supplemental Figure S1

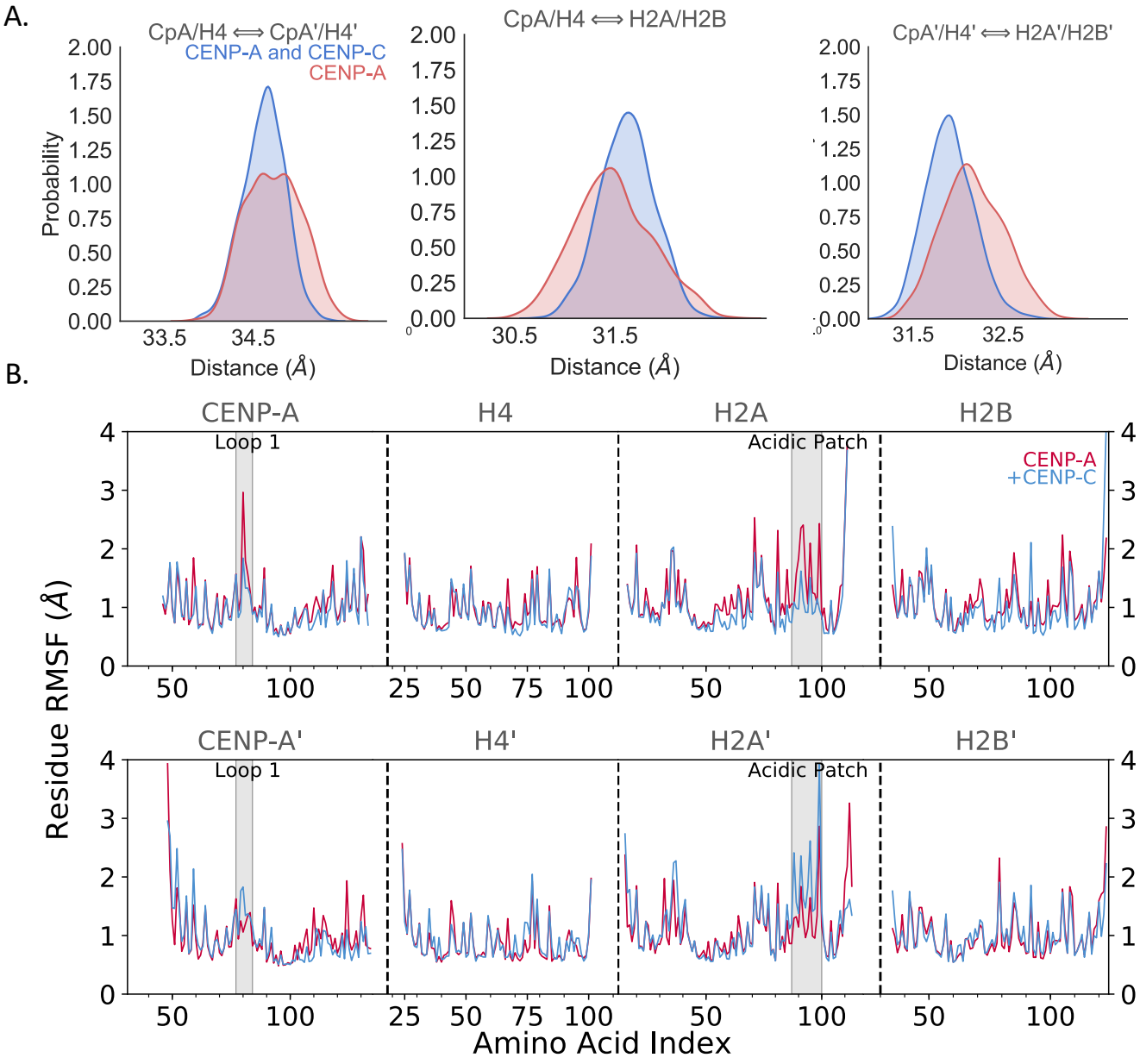

Supplemental Figure S2

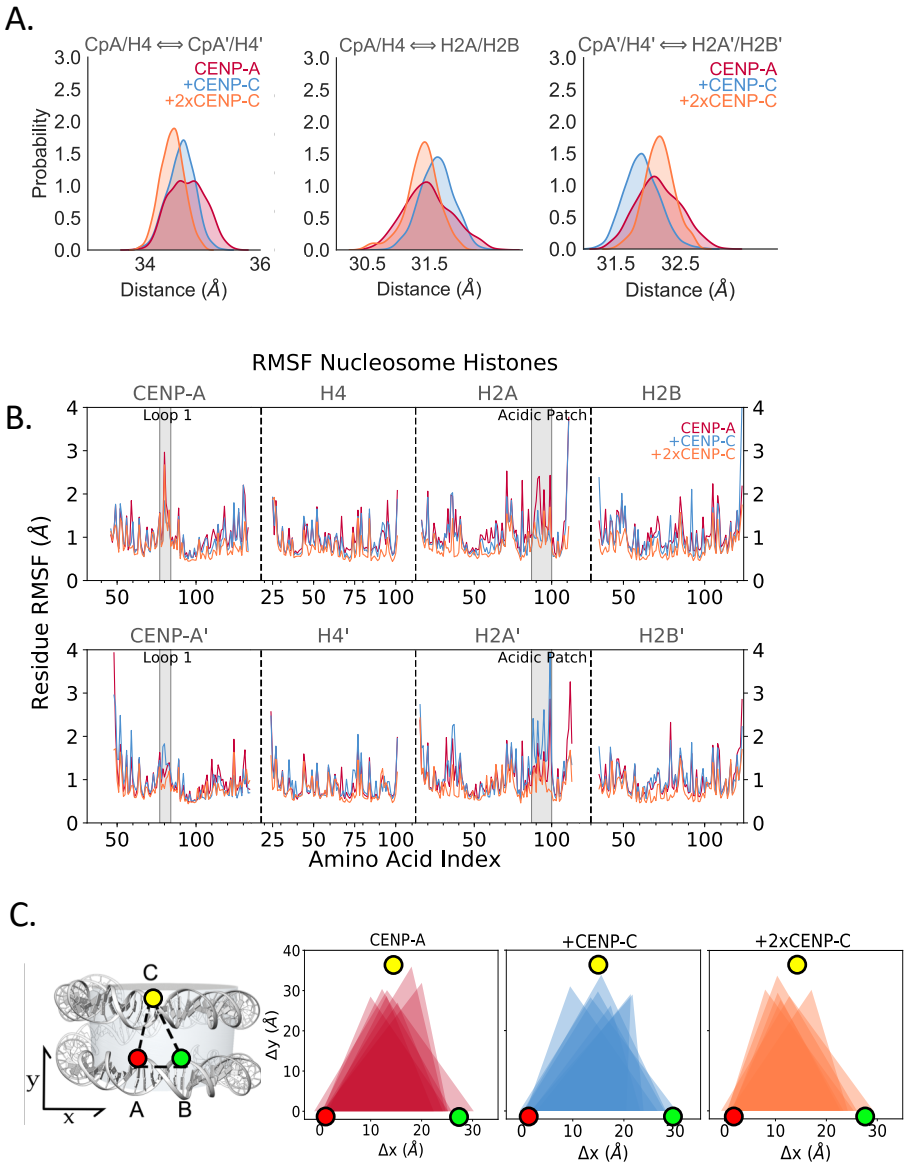

Supplemental Figure S3

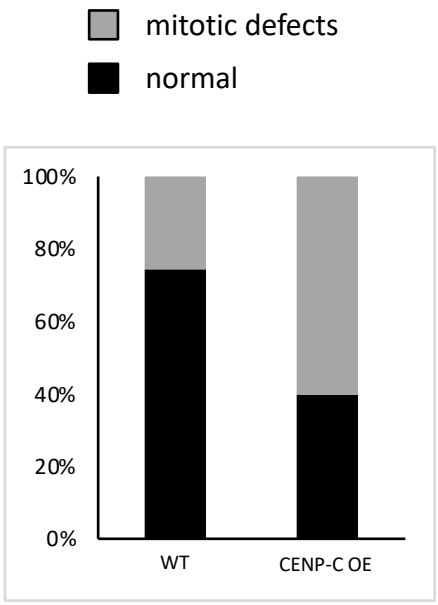

Supplemental Figure S4

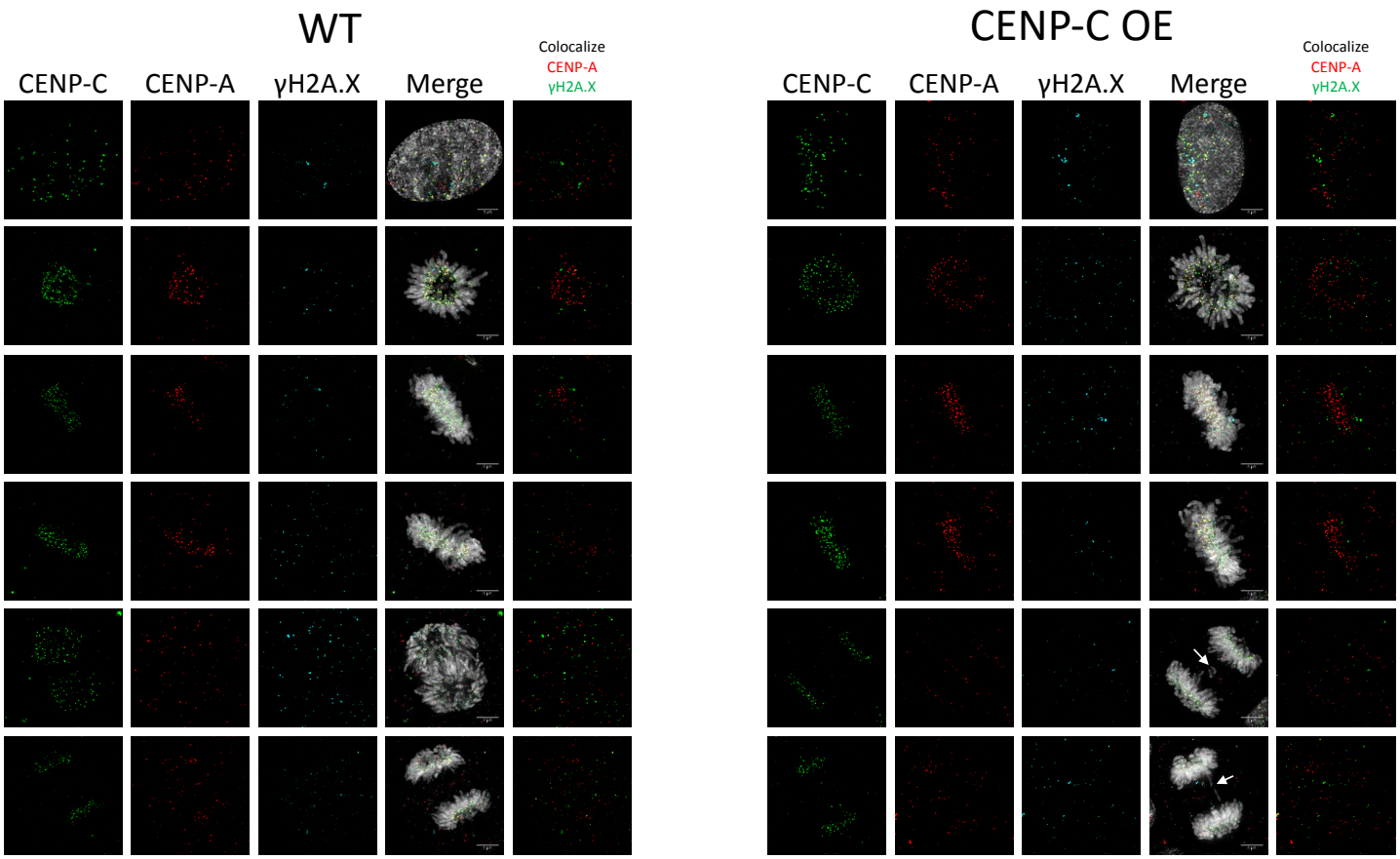

Supplemental Figure S5